https://doi.org/10.5194/egusphere-2026-4648
Preprint. Discussion started: 12 August 2026


# Quantifying trends and transitions in a Miocene benthic $\delta^{18}O$ stack

Bethany Hobart[1], Yuxin Zhou[2], Taehee Lee[3], Charles E. Lawrence[4], Lorraine E. Lisiecki[1]

[1]Earth Science Department, University of California, Santa Barbara, Santa Barbara, 93106, United States of America
[2]School of Earth and Atmospheric Sciences, Georgia Institute of Technology, Atlanta, GA 30332, USA
[3]Department of Earth, Environmental and Planetary Sciences, Brown University, Providence, RI 02912, USA
[4]Division of Applied Mathematics, Brown University, Providence, RI 02912, USA

*Correspondence to*: Lorraine E. Lisiecki (lisiecki@geol.ucsb.edu)

**Abstract.** Marine isotopic records from benthic foraminifera are central to understanding Miocene climate, but developing reliable Miocene age models that are consistent across sites has been challenging due ambiguities in biostratigraphy and magnetostratigraphy. Detailed chemostratigraphic alignment of globally distributed marine records can assist in comparing paleoclimate proxy records and their proposed forcing mechanisms. We present a continuous benthic $\delta^{18}O$ stack (average) across the Miocene based on alignment of published records from 24 sites. Stack estimates of global mean benthic $\delta^{18}O$ changes may improve reconstructions of Miocene ice volume change and deep-sea cooling and help distinguish between causal mechanisms. We estimate the rate of change in the global stack's benthic $\delta^{18}O$ throughout the Miocene as well as the amplitude of abrupt transitions associated with the onset of the Miocene Climatic Optimum (MCO) and the Middle Miocene Climatic Transition (MMCT). We find that the global stack's change in benthic $\delta^{18}O$ across the abrupt onset of the MCO at ~16.9 Ma is 0.27‰, which is about half the amplitude recorded in the deep Eastern Equatorial Pacific (EEP) and in the CENOGRID splice (Westerhold et al., 2020). We additionally find the total change in stack benthic $\delta^{18}O$ across the Miocene is 0.82‰, which is 15% less than in the CENOGRID splice.

## 1 Introduction

The Miocene epoch (23.03 – 5.33 Ma) was a dynamic period in Earth's climate history, characterized by extended periods of glaciation interrupted by an interval of global warmth known as the Miocene Climatic Optimum (MCO) from ~16.9 – 14.7 Ma. While the Miocene has been suggested as an analogue for future climate due to its warmer temperatures and elevated $pCO_2$, the highly variable conditions of the Miocene have proven particularly difficult to reconcile with climate models (Krapp and Jungclaus, 2011; Micheels et al., 2011; Herold et al., 2011, 2012; Bradshaw et al., 2012, 2014; Goldner et al., 2014; Burls et al., 2021). Marine isotopic records from calcareous microfossils play a key role in our understanding of Miocene climate. In particular, the oxygen isotope ratio, $\delta^{18}O$, of benthic foraminifera (henceforth, benthic $\delta^{18}O$) is interpreted as a proxy for global changes in deep ocean temperature and terrestrial ice volume. However, benthic $\delta^{18}O$ measured in individual sediment cores can also be affected by spatial variability in deep water temperature and salinity (e.g., Zhou et al., 2024) as well as disturbances of the sedimentary archive. Here we use detailed stratigraphic alignment of globally distributed benthic $\delta^{18}O$

records to construct a stack to better estimate global mean change across the Miocene for comparison with proposed tectonic, biogeochemical, oceanographic, or orbital forcing mechanisms.

We present a continuous Miocene benthic $\delta^{18}O$ stack which averages data from 24 globally distributed sites using revised age models for each record based on alignment to the CENOGRID benthic $\delta^{18}O$ splice (Westerhold et al, 2020). We hypothesize that this stack more accurately reflects global mean changes in benthic $\delta^{18}O$ than the splices of individual benthic $\delta^{18}O$ records that have previously been used to characterize Miocene climate variability (e.g., De Vleeschouwer et al., 2017; Miller et al., 2020; Westerhold et al., 2020). To compare the new stack with previously published records, we measure the slope of benthic $\delta^{18}O$ change on million-year timescales and the amplitude of change across relatively rapid climate transitions, particularly the abrupt warming at the onset of the MCO and stepwise cooling at the end of the mid-Miocene Climatic Transition (MMCT).

## 2 Background

Overall, the Miocene is characterized by long-term global cooling punctuated by several major climate transitions, particularly during the middle Miocene. Among these were the MCO, representing a prolonged interval of global warmth and reduced ice volume, and the MMCT, during which Antarctic ice sheets expanded and global temperatures began to decline. These events mark some of the most significant climate reorganizations of the Neogene.

### 2.1 Climate evolution and forcing mechanisms of the middle Miocene

The MCO, from approximately 16.9 – 14.7 Ma (Steinthorsdottir et al., 2021), was the warmest period in the Neogene with $CO_2$ proxies suggesting atmospheric concentrations between 400 – 1000 ppm (Rae et al., 2021; Herbert et al., 2022; Hönisch et al., 2023) and models estimating global mean surface temperatures between 5.3 and 11.5 °C higher than modern (Burls et al., 2021). The MCO saw nearly ice-free conditions, with global mean sea level estimates of >60 m above modern (Miller et al., 2020) and a seasonally sea ice-free Arctic Ocean (Herold et al., 2011; Super et al., 2020). Antarctic ice extent still experienced orbital-scale variability during the MCO (Holbourn et al., 2022), with spectral analysis of benthic $\delta^{18}O$ indicating sensitivity to ~100- and 405-kyr eccentricity cycles (Liu et al., 2024). The MCO also featured strong monsoon circulation, leading to more extreme precipitation variability and regional climate shifts, making terrestrial climates highly dynamic despite low global ice volumes (Galeotti et al., 2016; Liu et al., 2024).

The mechanisms that drove the relatively rapid warming at the start of the MCO are highly disputed. Until recently, many studies accepted that the MCO was likely triggered by large volumes of $CO_2$ outgassing associated with the emplacement of the Columbia River Basalt Group (CRBG) (Hodell and Woodruff, 1994), but new geochronology suggests the bulk of volcanism responsible for the CRBG occurred ~0.2 Myr after the onset of the MCO (Kasbohm et al., 2024). Other hypotheses attribute MCO warming to changes in East Antarctic Ice Sheet dynamics (e.g., Foster et al., 2012) or tectonic $CO_2$ degassing from increased rates of crustal production (Herbert et al., 2022). MCO climate may also have been influenced by changes in global ocean circulation. For example, new gateways began opening in the Southern Ocean ~34 – 21 Ma (Barker and Burrell,

https://doi.org/10.5194/egusphere-2026-4648
Preprint. Discussion started: 12 August 2026


1977; Toggweiler and Bjornsson, 2000; Lagabrielle et al., 2009) and in the Arctic as early as 25 Ma, resulting in a fully ventilated Arctic Ocean by ~17.5 Ma (Wright and Miller, 1996; Gladenkov and Gladenkov, 2004; Ehlers and Jokat, 2013; Hossain et al., 2021). Additionally, gateways to the Tethys Sea greatly constricted between roughly 17 – 14 Ma (Rögl, 1999; Simon et al., 2018).

The MCO was followed by the MMCT from ~14.7 – 13.8 Ma (Steinthorsdottir et al., 2021), during which benthic $\delta^{18}O$ values increased and climate variability decreased, suggesting a global cooling of ~3°C (Holbourn et al., 2007). Mean sea level fell an estimated 30 – 40 m during the MMCT, coincident with the development of a more stable East Antarctic Ice Sheet (Flower and Kennett, 1993; Holbourn et al., 2018; Miller et al., 2020). $pCO_2$ levels varied between 500-300 μatm from 14.25-13.53 Ma followed by a more stable value of ~320 μatm (Raitzsch et al., 2021). The MMCT and late Miocene are also associated with some of the greatest changes in the distribution of benthic foraminifera, likely due to a restructuring of meridional overturning circulation (Woodruff and Savin, 1989; Butzin et al., 2011).

Global ocean circulation was highly variable after the MCO and remains poorly understood, largely due to constrictions and closures of several important seaways. Late Miocene gateway changes include closure of the Panama Seaway in Central America ~14 – 4 Ma (Keigwin, 1982; Montes et al., 2015; O'Dea et al., 2016), final closure of the Tethys Sea by ~8 – 5 Ma (Rögl, 1999; Simon et al., 2018), and gateway constrictions near Indonesia ~8 – 4 Ma (Kuhnt et al., 2004; Christensen et al., 2017). Ambiguity remains as to when exactly these gateways closed; large dating uncertainties and differing definitions of a "closure" have potential to alter the timing of closure by millions of years, e.g., for the Panama Seaway (Keigwin, 1982; Haug et al., 2001; Montes et al., 2015; O'Dea et al., 2016; Kirillova et al., 2019).

Commonly proposed drivers of global cooling throughout the Miocene, particularly through the late Miocene, are atmospheric $CO_2$ decline possibly related to silicate weathering of the Himalayas (Raymo and Ruddiman, 1992; Ruddiman, 1997), weathering of mafic and ultramafic rocks in the tropics (Jagoutz et al., 2016; Macdonald et al., 2019), or changes in the rates of seafloor spreading and subduction (Herbert et al., 2022). Other hypotheses propose enhancement of the biological pump due to ash fertilization in the eastern Pacific Ocean (Wang et al., 2023) and/or decreased Pacific overturning (Ma et al., 2018).

## 2.2 Benthic isotopic records and their age models

Stable isotopes of benthic foraminifera are powerful tools for evaluating long-term variations in ocean circulation, global ice volume, and high-latitude surface temperatures (e.g., Shackleton et al., 1999; Lisiecki and Raymo, 2005; Pälike et al., 2006; Holbourn et al. 2018). The $\delta^{18}O$ signals recorded in carbonate shells of benthic foraminifera serve as a proxy for deep sea temperature and salinity as well as changes in the volume of land-based ice sheets. Given that deep water is globally well-mixed on the timescale of ocean circulation, the ice-volume component of benthic $\delta^{18}O$ changes is recorded nearly uniformly throughout the global ocean (e.g., Ma et al., 2018; Morée et al., 2021). However, differences in deep water temperature may introduce regional variability in benthic $\delta^{18}O$ that can contribute to uncertainty reconstructing global mean change and the alignment of globally distributed records (e.g., Zhou et al., 2024). Constructing a global benthic $\delta^{18}O$ stack (i.e., average) through stratigraphic alignment is one way to improve estimates of global mean change.

https://doi.org/10.5194/egusphere-2026-4648
Preprint. Discussion started: 12 August 2026


Marine isotopic records play a key role in our understanding of Miocene climate. For example, relatively abrupt $\delta^{18}O$ decreases during the MCO are evident in different oceans, supporting the global occurrence of this event: e.g., in the Central Equatorial Pacific (Woodruff and Savin, 1991), Southern Ocean (Billups et al., 2002), South China Sea (Holbourn et al., 2007), and Central Pacific Ocean (Kochhann et al., 2016). However, without the high-resolution stratigraphic correlation of isotope signals between sites, this abrupt shift in $\delta^{18}O$ may erroneously appear diachronous due to differences in sites' age models based on identification of biostratigraphic or magnetostratigraphic events in the recovered sediment (e.g. Abdul Aziz et al., 2003; Kissel et al., 2003; Kochhann et al., 2016). Biostratigraphic age estimates are affected by multiple sources of uncertainty, including sedimentary hiatuses, potential dissolution of nannofossils, and time transgressive first and last appearances of species (e.g. Hodell and Kennett, 1986; Rio et al., 1990; Backman et al., 2012). Stratigraphic correlation of magnetic reversals can also be ambiguous due to depositional hiatuses, and many marine sediment cores lack reliable magnetostratigraphy during the Miocene (e.g., Kochhann et al., 2016).

Age model comparisons reveal discrepancies between sites (e.g. Kochhann et al., 2016; Miller et al., 2017; Kasbohm, 2021; Westerhold et al., 2024). For example, comparisons of International Ocean Discovery Program (IODP) sites U1335 and U1336 illustrate the need for better age models by highlighting major inconsistencies between the magnetostratigraphic records for these neighboring sites (Kochhann et al., 2016). As expected for two sites that share similar paleogeography, U1335 and U1336 show strong agreement from ~18 to 16 Ma. However, sparse paleomagnetic data at Site U1335 result in poorly constrained magnetic reversal boundary identification beginning at chron C5Bn.2n (15.16 Ma; GTS12) and ambiguity in the younger portion of this record, with age uncertainties of >200 kyr. Gaps in paleomagnetic data such as these result in large uncertainties that pose problems for developing paleomagnetic age models for Miocene sediment cores. Furthermore, no single high-resolution benthic $\delta^{18}O$ record spans the whole of the Miocene without gaps. Resolving the causes and consequences of past climate change requires detailed stratigraphic alignments of available records to create consistent, synchronized age models between sites (Westerhold et al., 2024).

A few notable studies have characterized long-term climate change using mega-splices that meticulously interlace segments of high-resolution $\delta^{18}O$ and $\delta^{13}C$ data from different sites to construct a continuous record across some or all of the Cenozoic (De Vleeschouwer et al., 2017; Miller et al., 2020; Westerhold et al., 2020). Each $\delta^{18}O$ value in a mega-splice represents the value from a single location, which may be affected by local or regional climate responses that differ from global mean change. Furthermore, switching from one site to another in splices may create the appearance of global changes that are instead a product of spatial variability or imposed isotope offset corrections between coring locations (e.g., to correct for spatial gradients within the deep ocean). Here we use stacking to produce a continuous benthic $\delta^{18}O$ record across the Miocene which should be more representative of global change.

https://doi.org/10.5194/egusphere-2026-4648
Preprint. Discussion started: 12 August 2026


## 3 Construction of Miocene benthic $\delta^{18}O$ stacks

One advantage of stacking rather than splicing data is that stacking uses all available high-resolution Miocene benthic $\delta^{18}O$ records to construct a continuous global record that spans the whole epoch and combines information from multiple ocean basins. We constructed a global benthic $\delta^{18}O$ stack using the Bayesian stacking software BIGMACS (Lee et al., 2023), which generated revised and probabilistic age models for the stacked sites that are mutually consistent with respect to benthic $\delta^{18}O$ change. The BIGMACS algorithm iteratively aligns individual records to a target stack while estimating shift and scale parameters for each site to account for regional differences in mean $\delta^{18}O$ values (Appendix A). Gaussian process regression (GPR) in BIGMACS produces a continuous and smooth stack by averaging data aligned probabilistically; the relative influence of each individual record on the stack depends on its resolution (i.e., number of data points) in the vicinity of that point in the stack. The level of smoothing that occurs during stack construction depends on the resolution of the component records as well as their alignment uncertainty (Lee et al., 2023). BIGMACS also estimates a time-varying standard deviation for benthic $\delta^{18}O$ based on the distribution of aligned shifted-and-scaled $\delta^{18}O$ values across records and consideration of their alignment uncertainty. The output generated by BIGMACS includes 100 sample stacks together with 1000 sample aligned age models for each record in the stack (Hobart et al., 2026).

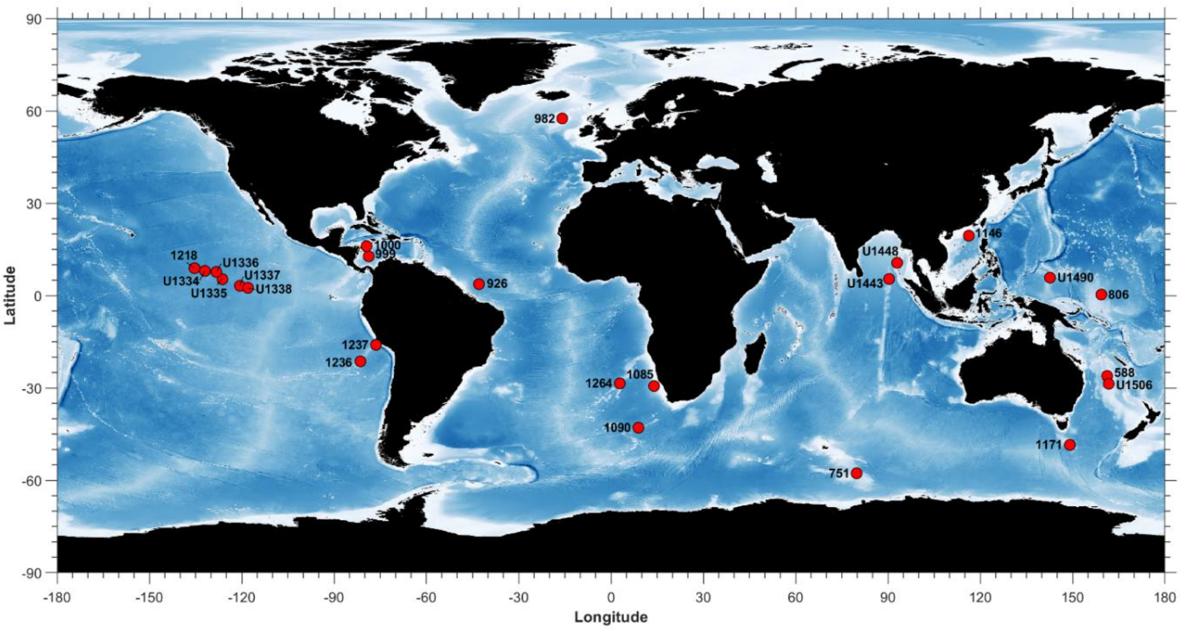


**Figure 1:** Map of the 24 Ocean Drilling Program (ODP) and International Ocean Discovery Program (IODP) sites from which data were used in this study. Blue shading illustrates modern seafloor bathymetry.

The Miocene stack includes high-resolution benthic $\delta^{18}O$ data from 24 globally distributed deep-sea drilling sites (Table 1, Fig. 1). To generate alignments of the individual records to the target stack with orbital scale-accuracy, we only include records

https://doi.org/10.5194/egusphere-2026-4648
Preprint. Discussion started: 12 August 2026


with an average sample spacing of less than ~10 kyr and with at least 400 kyr of continuous data. However, available high-resolution data provide uneven temporal and spatial coverage of the global ocean (Fig. 2). The stack does not include IODP Site U1505C (18° 55.0570' N, 115° 51.5370' E; water depth 2916.6 m) from the South China Sea because its average sample spacing is >10 kyr (Liu et al., 2024) and most of the stack construction was performed before its publication.

The age model of the stack and its aligned records are based on the CENOGRID mega-splice published by Westerhold et al. (2020), which we used as the initial alignment target in BIGMACS. The CENOGRID mega-splice incorporates previously published astrochronologies for individual records as well as additional tuning to the La2010b orbital solutions (Laskar et al., 2011) for some records. The $\delta^{18}O$ records and much of the astrochronology used in the Miocene portion of CENOGRID were originally published by Drury et al. (2017, 2021), Holbourn et al. (2014, 2015; 2018), and Liebrand et al. (2016). Subsequent analysis suggests the CENOGRID age model is impacted by a tuning error for Site U1337 between approximately 18-17 Ma with a maximum age shift of 300 kyr at ~18 Ma (Hilgen, 2025).

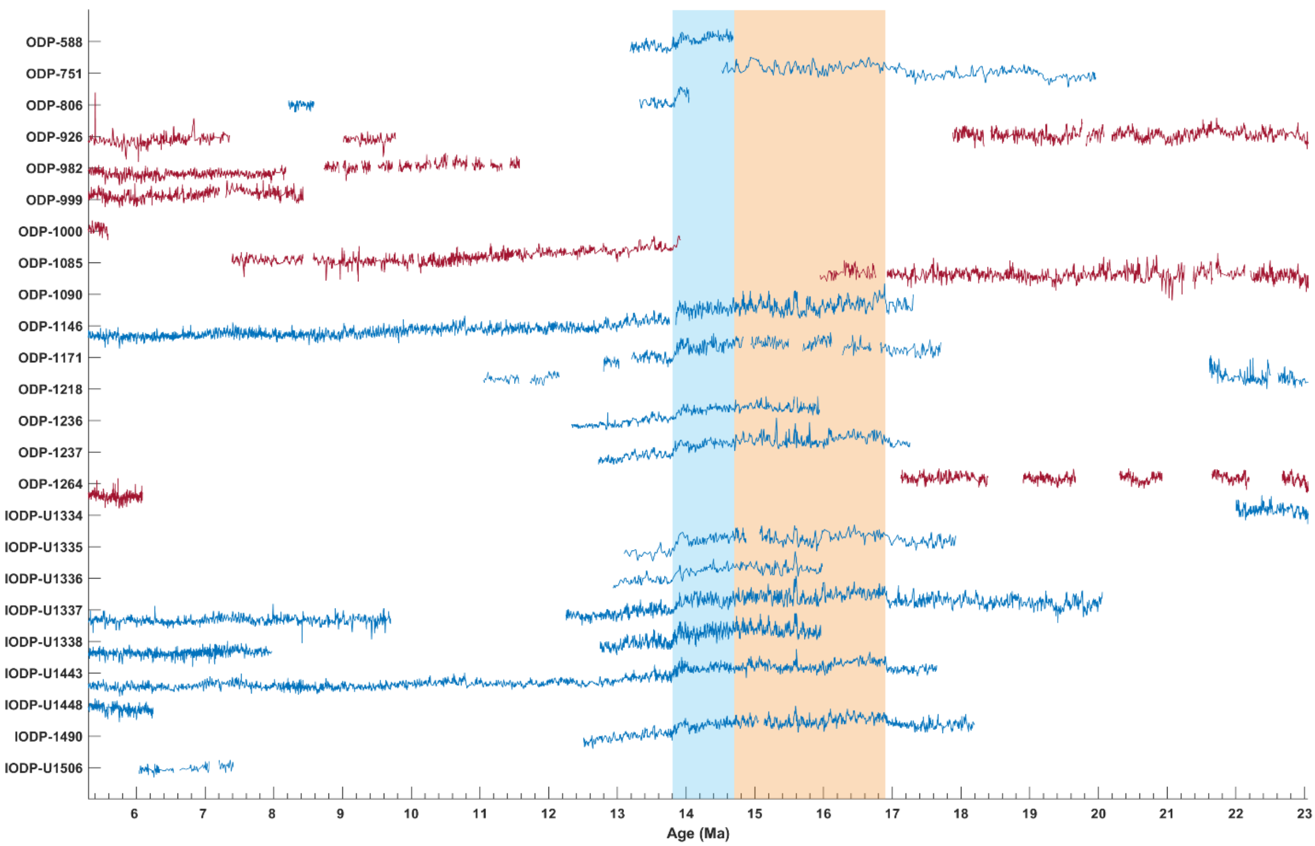


**Figure 2:** The benthic $\delta^{18}O$ records used in this study (Table 1) plotted on their revised age models after stratigraphic alignment, offset vertically for clarity. Available high-resolution data from the Atlantic Ocean (red) and the Pacific, Indian, and Southern Oceans (blue) provides uneven temporal and spatial coverage. The MMCT and MCO are shaded in blue and orange, respectively.

https://doi.org/10.5194/egusphere-2026-4648
Preprint. Discussion started: 12 August 2026


**Table 1:** Site locations and citations for benthic $\delta^{18}O$ records included in the stack.

| Site | Latitude | Longitude | Depth (m) | Range (Myr) | References |
|---|---|---|---|---|---|
| DSDP 588 | -26.1117 | 161.2267 | 2793 | 14.7 – 13.0 | Flower & Kennett (1993) |
| ODP 751 | -57.7261 | 79.8147 | 1810 | 20.0 – 14.5 | Miller et al. (2017) |
| ODP 806 | 0.3185 | 159.3610 | 2615 | 14.8-13.5 | Holbourn et al. (2018) |
| ODP 926 | 3.7190 | -42.9083 | 3936 | 13.8 – 4.9 | Shackleton and Hall (1997) |
| | | | | | Wilkens et al. (2017) |
| | | | | 23.1 – 17.9 | Pälike et al. (2006) |
| ODP 982 | 57.5167 | -15.8500 | 1395 | 11.6 – 8.2 | Andersson & Jansen (2003) |
| ODP 999 | 12.7440 | -78.7393 | 3405 | 8.4 – 5.3 | Bickert et al. (2004) |
| ODP 1000 | 16.0537 | -79.4590 | 1480 | 5.6 – 5.0 | Steph (2005) |
| ODP 1085 | -29.3744 | 13.9901 | 2329 | 13.9 – 7.4 | Westerhold et al. (2005) |
| ODP 1090 | -42.9136 | 8.8998 | 3702 | 23.1 – 15.9 | Billups et al. (2002, 2004) |
| ODP 1146 | 19.4567 | 116.2729 | 2091 | 17.3 – 5.1 | Holbourn et al. (2021) |
| ODP 1171 | -48.4999 | 149.1117 | 2148 | 11.1 – 17.7 | Shevenell & Kennett (2004) |
| | | | | | Holbourn et al (2024) |
| ODP 1218 | 8.8896 | -135.3667 | 4828 | 23.1 – 21.6 | Tripati et al. (2006) |
| ODP 1236 | -21.3590 | -81.4361 | 1323 | 15.6 – 12.2 | Tiedemann et al. (2007) |
| ODP 1237 | -16.0070 | -76.3781 | 3212 | 17.1 – 12.7 | Holbourn et al. (2007) ; |
| | | | | | Tiedemann et al. (2007) |
| ODP 1264 | -28.5325 | 2.8455 | 2507 | 6.1 – 5.0 | Liebrand et al. (2016) |
| IODP U1334 | 7.9993 | -131.9732 | 4799 | 23.1 – 22.0 | Beddow et al. (2016) |
| IODP U1335 | 5.3123 | -126.2835 | 4328 | 19.8 – 14.9 | Kochhann et al. (2016) |
| IODP U1336 | 7.7011 | -128.2542 | 4286 | 16.0 – 12.9 | Voigt et al. (2015) |
| IODP U1337 | 3.1706 | -120.5879 | 4463 | 8.3 – 5.9 | Kochhann et al. (2016) |
| | | | | 20.0 – 14.8 | Drury et al. (2017) |
| IODP U1338 | 2.5078 | -117.9696 | 4200 | 8.2 – 3.6 | Lyle et al. (2019) |
| | | | | 16.0 – 12.7 | Holbourn et al. (2014) |
| IODP U1443 | 5.3835 | 90.3618 | 2940 | 9.0 – 5.0 | Bolton et al. (2021) |
| | | | | 17.7 – 13.6 | Kochhann et al. (2021) |
| IODP U1448 | 10.6353 | 93.0001 | 1098 | 6.2 – 5.0 | Jöhnck et al. (2020) |
| IODP U1490 | 5.8158 | 142.6544 | 2341 | 12.5 – 18.2 | Holbourn et al. (2024) |
| IODP U1506 | -28.6620 | 161.7404 | 1495 | 6.0 – 7.4 | Gastaldello et al., (2023) |

To achieve reasonable run times for BIGMACS, five separate stacks were constructed using 4-Myr overlapping time intervals across the Miocene (Fig. A1). To create one continuous record (Figure 3), we apply offsets to four of the segments by subtracting the difference in the mean of the overlapping portion of the stack segments. Additionally, we generate a smooth transition between the stack segments by applying a transitional weighted mean for the stack value and its standard deviation across the overlap windows. See Appendix A for a detailed description. We additionally constructed a regional stack for the Eastern Equatorial Pacific (EEP) from 18 – 13 Ma (Fig. 4) using sites IODP sites U1335, U1336, U1337, and U1338, which have high-resolution data spanning much of the middle Miocene (Holbourn et al., 2014; Voigt et al., 2015; Kochhann et al.,

https://doi.org/10.5194/egusphere-2026-4648
Preprint. Discussion started: 12 August 2026


2016; Drury et al., 2017; Lyle et al., 2019). This allows us to evaluate how the middle Miocene portion of CENOGRID splice, which uses individual records from the EEP, compares to a stack of available records from the same region.

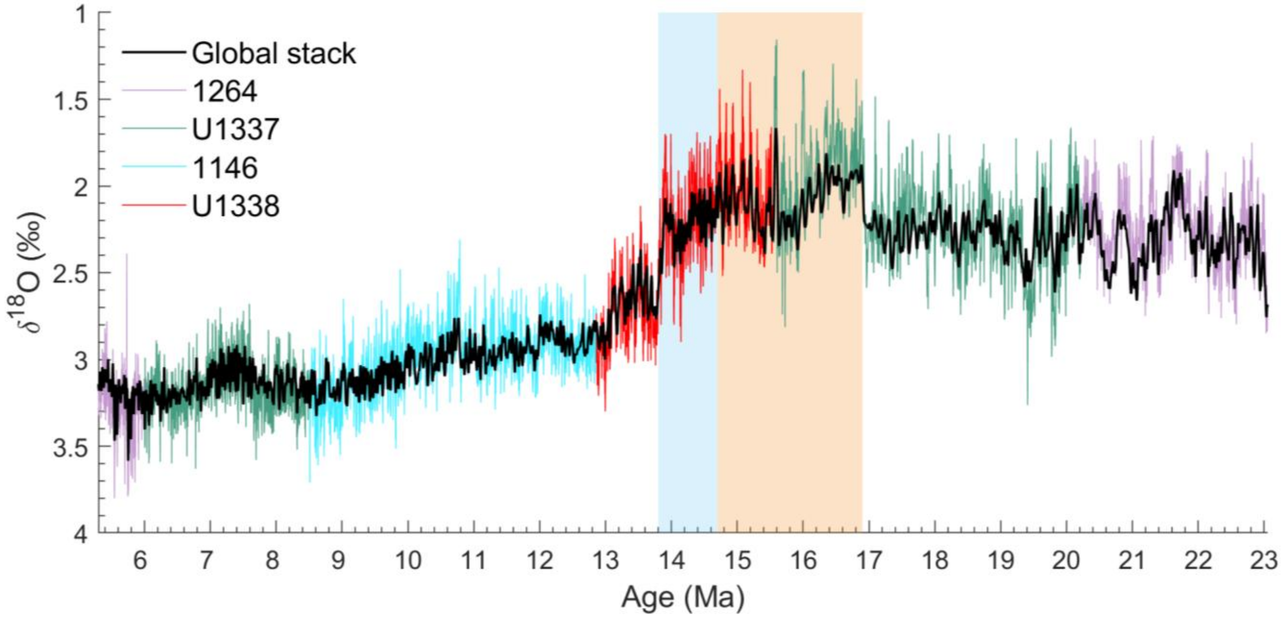


**Figure 3:** Comparison of global stack and CENOGRID mega-splice. This study's global benthic $\delta^{18}O$ stack (black) is shown with a species correction of +0.64‰ to match that used in the CENOGRID splice (multi-colored, Westerhold et al., 2020). Colors show data from different core sites in the CENOGRID splice, with a 20-kyr smoothing as applied by Westerhold et al. (2020). The MMCT and MCO are represented by the shaded blue and orange regions, respectively.

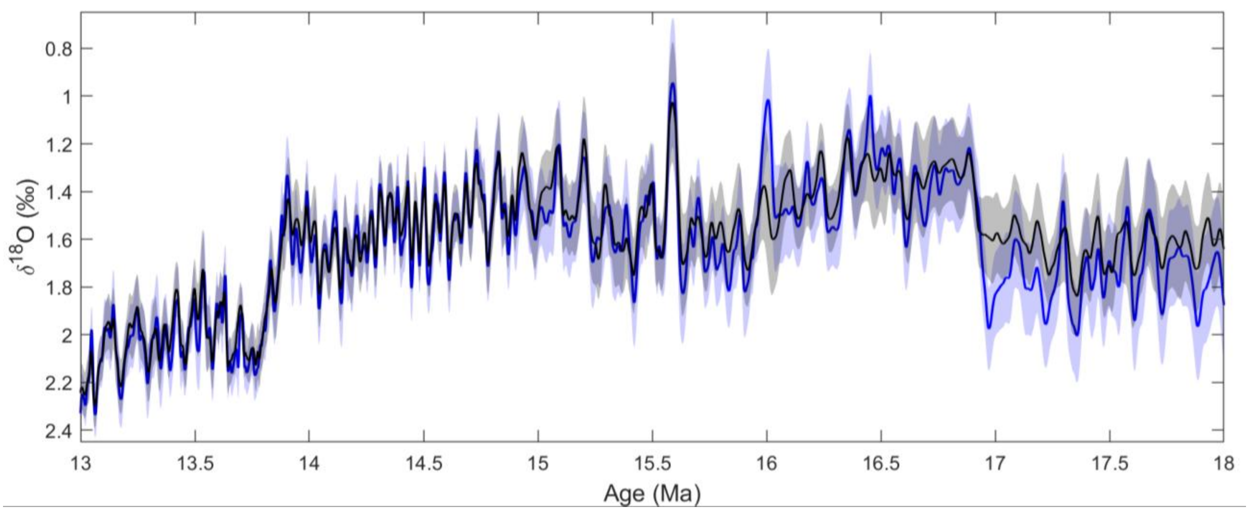


**Figure 4:** Middle Miocene portion of the global benthic $\delta^{18}O$ stack (black) and the regional stack of EEP sites (blue). Shaded regions represent the one-standard deviation spread of $\delta^{18}O$ values estimated by BIGMACS (black and blue, respectively).

https://doi.org/10.5194/egusphere-2026-4648
Preprint. Discussion started: 12 August 2026


## 4 Quantifying stack trends and transitions

### 4.1 Transitions

We use the term transitions to describe relatively abrupt changes in the mean value of benthic $\delta^{18}O$ occurring over timescales of ~100 kyr. Quantifying the duration and amplitude of major transitions in benthic $\delta^{18}O$ assists with answering questions about the magnitude of ice volume and temperature changes occurring at those times. Here we focus on the large and relatively rapid climate transitions occurring at the start of the MCO and the end of the MMCT.

Bayesian change point analysis probabilistically identifies the occurrence of major shifts in a time series (Ruggieri and Lawrence, 2014), making it a good choice for identifying important climate transitions such as the MCO and MMCT. To get age estimates for these rapid shifts in the global and EEP stacks as well as the CENIGRID splice, we analyzed the onset of the MCO and the end of the MMCT using time windows of 17.1 – 16.7 Ma and 14.05 – 13.65 Ma, respectively (Fig. 5, Table 2). These age estimates all rely on benthic $\delta^{18}O$ alignments to the CENOGRID splice (Westerhold et al., 2020). For the global stack, the algorithm estimated change points at 16.94 Ma and 16.88 Ma for the beginning and end of the MCO onset and at 13.88 Ma and 13.80 Ma for the abrupt change at the end of the MMCT. 95% confidence intervals (Table 2) for the timing of the MCO onset and the MMCT and their durations are based on 1000 Monte Carlo simulations generated by the change point software.

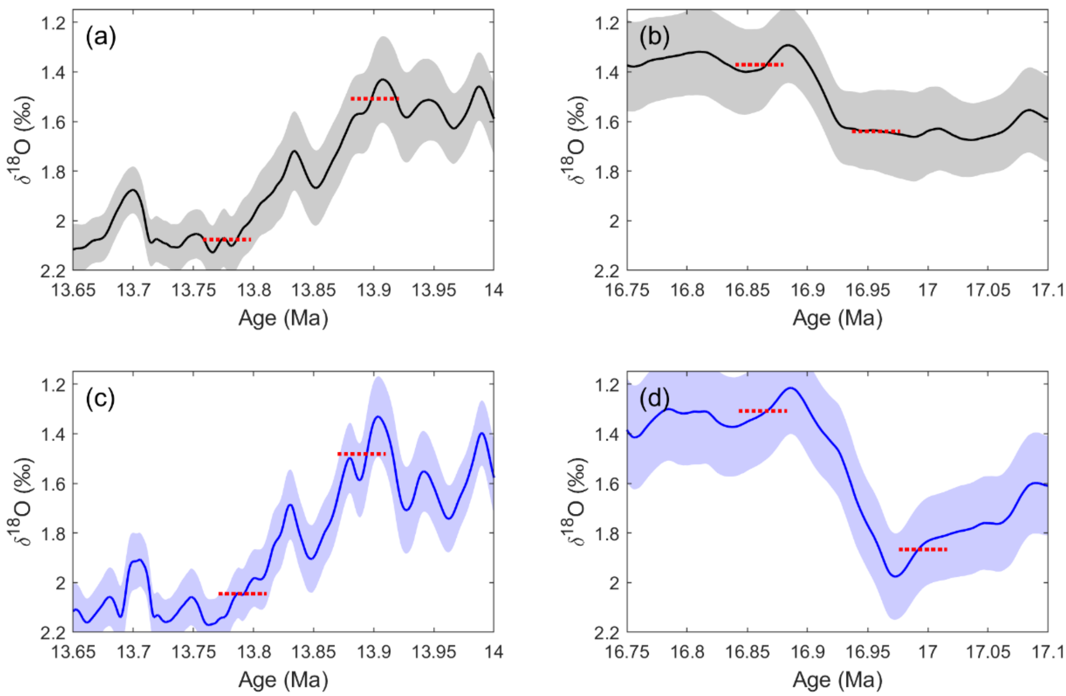


**Figure 5**: Abrupt transitions for the MMCT (a and c) and the MCO onset (b and d) in the global (black) and regional EEP (blue) stacks, with shading showing the standard deviation for $\delta^{18}O$ values. Amplitudes are measured as the between average values across 40-kyr sampling windows before and after each transition (red dotted lines) based on change point identification (Table 2).

https://doi.org/10.5194/egusphere-2026-4648
Preprint. Discussion started: 12 August 2026


**Table 2:** Change point ages and the associated benthic $\delta^{18}O$ change across the start of the MCO and the end of the MMCT for the global stack, the EEP stack, and the CENOGRID splice (Westerhold et al., 2020). Values in square brackets denote 95% confidence intervals.

| | Global stack | EEP stack | CENOGRID |
|---|---|---|---|
| MCO onset | | | |
| Start (Ma) | 16.94 [16.93 16.95] | 16.98 [16.97 16.99] | 16.97 [16.97 16.98] |
| End (Ma) | 16.88 [16.87 16.89] | 16.88 [16.88 16.91] | 16.88 [16.88 16.89] |
| $\delta^{18}O$ change (‰) | -0.269 [-0.212 -0.333] | -0.558 [-0.414 -0.720] | -0.609 |
| MMCT end | | | |
| Start (Ma) | 13.88 [13.87 13.90] | 13.87 [13.86 13.88] | 13.89 [13.89 13.90] |
| End (Ma) | 13.80 [13.78 13.81] | 13.81 [13.80 13.82] | 13.81 [13.79 13.82] |
| $\delta^{18}O$ change (‰) | 0.567 [0.526 0.599] | 0.563 [0.492 0.611] | 0.794 |

The amplitudes of benthic $\delta^{18}O$ change across the transitions (Table 2) are measured as the change in the mean $\delta^{18}O$ value between two 40-kyr sampling windows on either side of the change point age for the start and end of the transition (dotted red lines in Fig. 5). Confidence intervals for amplitude changes were estimated based on means across the same time windows for 100 different sample stacks generated by BIGMACS (Hobart et al., 2026).

While the timing and duration of these two transitions are nearly identical in the EEP and global stacks, the amplitude of change for the MCO onset in the EEP stack, -0.56‰ [95% CI: -0.41 -0.72], is approximately twice that of the global stack, -0.27‰ [95% CI: -0.21 -0.33], a statistically significant difference. In contrast, the EEP and global stacks have approximately equal amplitudes during the MMCT, with estimates of 0.56‰ for the EEP and 0.57‰ for the global stack. The CENOGRID splice is similar to the EEP stack for the MCO onset (-0.61‰) but has a larger amplitude than the EEP stack at the end of the MMCT (0.79‰). Similarity between the CENOGRID splice and the EEP stack is expected because the splice uses EEP sites during the middle Miocene, but differences between sites and/or smoothing during stack construction could decrease the amplitudes observed in the stack.

### 4.2 Trends

Gradual cooling trends across the Miocene were quantified by calculating the rate of change of benthic $\delta^{18}O$ through time. Because the MCO and MMCT disrupt the overall cooling trend throughout the Miocene, we have separated the Miocene into several different intervals for which we calculate the linear slope of benthic $\delta^{18}O$ change: the early Miocene (23.03 – 16.94 Ma), the MCO (16.88 – 14.7 Ma), the MMCT (14.7 – 13.88 Ma), a post-MMCT interval (13.8 – 12.5 Ma), a middle-late Miocene interval (12.5 – 9 Ma) and a latest Miocene interval (9 – 5.33 Ma) (Table 3). Trends were calculated based on weighted least square linear regression using MATLAB's 'fitlm' function (The Mathworks Inc., 2024), with weights defined as the inverse of the squared standard deviation for stack $\delta^{18}O$. CENOGRID and IODP Site U1505C trends were calculated across the same time windows using unweighted $\delta^{18}O$ values on their original age models.

**Table 3:** Slope estimates in (‰ $Myr^{-1}$) for different Miocene time windows in the global stack, the EEP stack, CENOGRID (Westerhold et al., 2020), and IODP Site U1505C (Liu et al., 2024). Slope uncertainty is given as one standard error.

| | Age range (Ma) | Global stack | EEP stack | CENOGRID | U1505C |
|---|---|---|---|---|---|
| early Miocene | 23.03 – 16.95 | -0.010 ± 0.001 | | -0.007 ± 0.002 | |
| MCO | 16.89 – 14.70 | 0.070 ± 0.004 | 0.071 ± 0.005 | 0.110 ± 0.012 | 0.105 ± 0.031 |
| MMCT | 14.70 – 13.89 | 0.171 ± 0.015 | 0.165 ± 0.018 | 0.216 ± 0.046 | 0.185 ± 0.121 |
| post-MMCT | 13.79 – 12.50 | 0.291 ± 0.007 | | 0.278 ± 0.018 | 0.362 ± 0.042 |
| mid-to-late Mio. | 12.50 – 9.0 | 0.080 ± 0.001 | | 0.070 ± 0.004 | 0.088 ± 0.011 |
| latest Miocene | 9.0 – 5.33 | 0.020 ± 0.001 | | 0.011 ± 0.003 | |

The early Miocene is the only interval over which the global stack exhibits a negative $\delta^{18}O$ trend (indicative of warming), although this is also one of the most gradual rates of change in the Miocene (Table 3). The most rapid rate of change, 0.291 ± 0.007 ‰/Myr occurs from 13.8 – 12.5 Ma, just after the stepwise cooling at the MMCT (Fig. 6); this post-MMCT cooling has also been documented by Kryolov et al. (2008) and Lear et al. (2015). The next largest cooling trend occurs during the MMCT from 14.70 – 13.88 Ma with a change of 0.171 ± 0.015 ‰/Myr, excluding the abrupt change from 13.89-13.79 Ma. The remaining trends are much more gradual. The EEP stack shows similar trends to the global stack where they overlap during the MCO and MMCT.

The CENOGRID cooling rates during the MCO and MMCT (0.11 and 0.22 ‰/Myr, respectively) are both larger than the trends of 0.07‰/Myr (MCO) and 0.17‰/Myr (MMCT) in the stacks. In contrast, the global stack has slightly greater rates of cooling than CENOGRID after the MMCT, although the slope differences for the MMCT and post-MMCT time intervals are not statistically significant. IODP Site U1505C (Liu et al., 2024) has consistently stronger cooling rates than the global stack (Table 3; Fig. 6). The largest differences are during the post-MMCT interval and in the early Miocene (21-16.95 Ma), during which U1505C shows a cooling trend of 0.023 ± 0.015 ‰/Myr, instead of the warming trend observed in the global stack and CENOGRID splice.

To estimate the total change in benthic $\delta^{18}O$ across the Miocene, we take the difference between the first 0.5 Myr of the Miocene (23.03-22.53 Ma) and the last 0.5 Myr (5.83-5.33 Ma). The global stack increases by 0.823 ± 0.008 ‰ (one standard error) across the Miocene whereas the CENOGRID splice increases by 0.967 ± 0.018 ‰, 17% more than the stack. To compare with IODP Site U1505C, we calculate the change in mean values for 21-20.5 Ma and 6.75-6.25 Ma in each record. The results for the global stack and CENOGRID splice, 0.817 ± 0.010 ‰ and 0.959 ± 0.012 ‰, respectively, are similar to their change across the whole Miocene. In contrast, IODP U1505C increases by 1.184 ± 0.048 ‰ from 21 Ma to 6.25 Ma, which is 45% more than the change in the global stack.

https://doi.org/10.5194/egusphere-2026-4648
Preprint. Discussion started: 12 August 2026


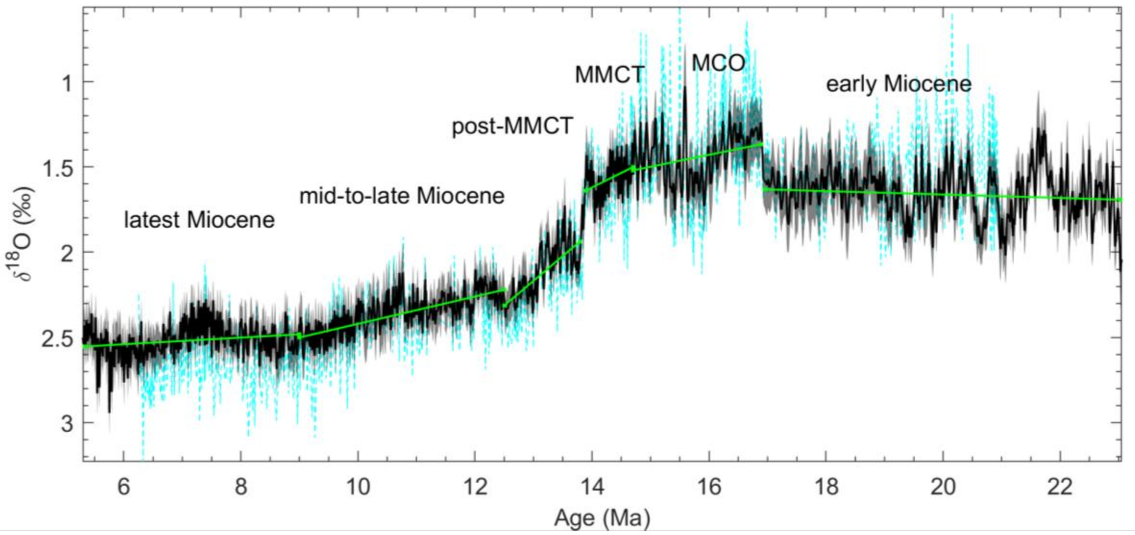


**Figure 6:** The global Miocene stack (black) and its standard deviation (gray shading) compared to benthic $\delta^{18}O$ values from IODP Site U1505 with +0.35 ‰ offset (dashed cyan line; Liu et al., 2024). Green line segments show best-fit linear trends for the labelled time intervals in the stack (Table 3).

## 5 Discussion

Age estimates for the MCO and MMCT are consistent between the global stack, EEP stack, and CENOGRID; the largest age difference in change point identification is 40 kyr for the onset of the MCO between the global and EEP stacks. Stratigraphic alignment uncertainty or regional differences in benthic $\delta^{18}O$ are the most likely explanations for this difference because the age models for both stacks are derived from the CENOGRID splice (Westerhold et al., 2020).

While our alignment methodology keeps the timing of the MCO and MMCT of the stacks consistent with CENOGRID, there are important differences in the amplitude of change between records. Similarity between CENOGRID and the EEP stack can largely be explained by CENOGRID's use of sites U1337 and U1338 during the middle Miocene, both located in the EEP. Despite the smoothing applied to our regional EEP record during the stacking process, the $\delta^{18}O$ change associated with the MCO onset is only 0.05 ‰ less in the EEP stack than in CENOGRID. For the MMCT transition, however, stack smoothing or differences between EEP sites decreased the amplitude of the EEP stack relative to IODP site U1338, as used in the CENOGRID splice.

Comparing the amplitudes of the EEP and global stacks during the MCO onset suggests that the changes in the EEP during the MCO are not representative of global mean change. However, the "global" stack is also not truly a global average due to a lack of high-resolution data from the Atlantic Ocean during the MCO (Fig. 2). Therefore, stack comparisons during the MCO are primarily reflecting differences between the EEP sites and other parts of the Pacific Ocean. IODP site U1337, which provides most of the data in the EEP stack during the MCO onset, had a paleo-depth of ~4000-3500 m (Holbourn et al., 2022)

https://doi.org/10.5194/egusphere-2026-4648
Preprint. Discussion started: 12 August 2026


and was much deeper than most of the other Pacific cores included in this study, which have a modern mean depth of ~2000 m. The greater depths of EEP sites and their higher benthic $\delta^{18}O$ values before the MCO may indicate that they were bathed by a larger proportion of cold, dense Antarctic Bottom Water (AABW) water than other Pacific sites at that time, perhaps related to the development of modern-like Circumpolar Deep Water (CDW) beginning in the middle Miocene (Evangelinos et al., 2024). Carbonate dissolution or diagenetic alteration may also be contributing factors (Edgar et al., 2013; Poirier et al., 2021). Another concern is that the global and EEP stack signals might each primarily reflect responses from their highest resolution records. A more detailed examination of differences in the amplitude of MCO onset across all available sites could help distinguish between these explanations.

The nearly identical amplitudes of change at the MMCT in the EEP and global stacks, despite differences at the onset of the MCO, suggest a shift in Pacific deep water circulation during the MCO which led to the EEP benthic $\delta^{18}O$ and $\delta^{13}C$ values becoming more similar to the rest of the Pacific (Cramer et al., 2009; Holbourn et al., 2022). Model simulations suggest that most of the global ocean below 1500 m was filled by a single southern-sourced deep water mass during the MCO (Herold et al., 2012). The redistribution of benthic microfauna in the middle Miocene is another indication of changing deep water currents (Dickens and Owen, 1999; Lyle et al., 2019). Across the MMCT, increasing benthic $\delta^{13}C$ gradients are indicative of a progressive deep Pacific stratification following the MCO (Holbourn et al., 2022). However, similar values in the EEP and global stacks during and just after the MMCT (Figure 4) suggests that divergence between the deep EEP and other Pacific sites occurred after 13 Ma.

The Miocene also saw several other changes in meridional overturning circulation which could have regional impacts on benthic $\delta^{18}O$. For example, the $\varepsilon_{Nd}$ water mass tracer exhibits a long-term decrease at the Walvis Ridge from 23 – 11 Ma, suggesting an increase in the contribution of northern component water to deep waters in the south Atlantic from the early to middle Miocene (Thomas and Via, 2007). A permanent divergence in benthic $\delta^{13}C$ signatures between the deep North Atlantic and Pacific developed during the MMCT and early-late Miocene (~13.9 – 9 Ma) (Cramer et al., 2009; Butzin et al., 2011; Tian et al., 2013). This change is attributed to well-ventilated northern deep water playing a stronger role in meridional overturning circulation through increased Atlantic salinification following tropical gateway closures, and an increased supply of cold water from Nordic seas (Steinthorsdottir et al., 2021). Tropical gateway closures, which imposed a longer deep water route between the Atlantic and Pacific Oceans, may also have led to increased deep Pacific residence times (Holbourn et al., 2024).

Although data coverage for the global stack does not consistently include sites from all major ocean basins, it likely provides a better estimate of trends in global mean benthic $\delta^{18}O$ than the CENOGRID mega-splice. The trends estimated for the stacks have relatively small uncertainties (Table 2), and orbital-scale GPR smoothing during the stacking process should also have little impact on estimates of million-year trends. Across the whole Miocene, the global stack suggests that the amount of cooling and/or ice volume growth affecting benthic $\delta^{18}O$ is 0.14 ‰ less than inferred from the CENOGRID splice, and 0.37 ‰ less global change is inferred from the stack between 21-6.25 Ma than at IODP Site U1505C in the South China Sea. Long-term differences between the global stack and the CENOGRID splice across the Miocene may result from the effects of splicing

https://doi.org/10.5194/egusphere-2026-4648
Preprint. Discussion started: 12 August 2026


records from different locations. Differences between the global stack and IODP site U1505C may be explained by tectonic and ocean circulation changes in the South China Sea that induced regional benthic $\delta^{18}O$ changes.

Improved estimates of mean benthic $\delta^{18}O$ changes from the global stack may offer insight into the mechanisms that influenced global climate across the Miocene. However, the new global stack is still based on a relatively small number of high-resolution records at any point in time and, thus, not truly representative of global mean benthic $\delta^{18}O$. Nonetheless, comparison between the stacks, splice, and individual records demonstrates uncertainty in the amplitudes of trends and transitions in Miocene benthic $\delta^{18}O$, likely associated with the regional effects of deep water circulation changes.

## 6 Conclusions

This study assesses Miocene climate change using a new, continuous benthic $\delta^{18}O$ stack. Through stratigraphic alignment of high-resolution benthic $\delta^{18}O$ data, our stack resolves age discrepancies between previously published age models of individual records and should more accurately represents global benthic $\delta^{18}O$ change than existing mega-splices. However, a truly global compilation will require high-resolution Atlantic benthic $\delta^{18}O$ records spanning the MCO.

By comparing a global and regional stack across the MCO, we observe that the amplitude of benthic $\delta^{18}O$ change in the EEP was twice as large as in the global (although mostly Pacific) stack during the onset of the MCO. We propose that this discrepancy results from the development of modern-like lower CDW formation that resulted in AABW bathing the deep EEP sites before the MCO (Holbourn et al., 2022). In contrast, similar amplitudes of change for the two stacks during the MMCT suggests more homogeneous Pacific deep water at that time, potentially caused by decreased overturning and weakened southern-sourced deepwater formation (Ma et al., 2018). With respect to long-term trends, the global stack exhibits a smaller rate of benthic $\delta^{18}O$ increase (cooling) in the early-to-middle Miocene (23-13.9 Ma) than the CENOGRID splice but a greater rate of increase from 13.7-5.33 Ma. Across the whole Miocene, the global stack decreases by 0.823 ± 0.008 ‰, compared to 0.967 ± 0.025 ‰ in the CENOGRID splice.

## 7 Appendix A

To speed up run times in BIGMACS, five separate stacks were constructed for the intervals of 23 – 19 Ma, 19.5 – 15.5 Ma, 16 – 12 Ma, 12.5 – 8.5 Ma, and 9 – 5 Ma (Fig. A1). When iteratively aligning individual records to the target stack, BIGMACS applies record-specific shift and scale constants to the data from each site to account for spatial variability in the ocean and laboratory- or species-specific offsets. The shift parameter is a constant offset applied to each record based on the average $\delta^{18}O$ difference between overlapping regions of that record and the stack, and the scale parameter is estimated based on the standard deviation of each $\delta^{18}O$ record. The mean and scaling of each resulting stack reflects the average values of its component records. Offsets between stack segments can occur because each stack includes a different set of sites. To join the stack segments, we apply constant offsets to four of the segments by subtracting the difference in the mean of the overlapping portion

https://doi.org/10.5194/egusphere-2026-4648
Preprint. Discussion started: 12 August 2026


of the stack segments. Measured offsets between successive segments are 0.2554‰ for the overlap window 8.5-9 Ma, -0.0462‰ for 12-12.5 Ma, 0.0555‰ for 15.5-16 Ma, and 0.0346‰ for 19-19.5 Ma. We shift the first, second, fourth and fifth stack segment based on these offsets to match the stack segment spanning 16 – 12 Ma in the middle Miocene.

To create a smooth transition between stack segments, the stack $\delta^{18}O$ values within the 500-kyr overlap windows were calculated by averaging the two overlapping segments using a weighting function that linearly varies from 100% to 0% for each segment across the overlap window. The standard deviations for the $\delta^{18}O$ stacks were similarly calculated as weighted means transitioning from 100% to 0% across the overlap window. This yields one continuous record spanning the whole of the Miocene with smooth transitions where the shorter stacks were stitched together (Fig. 3).

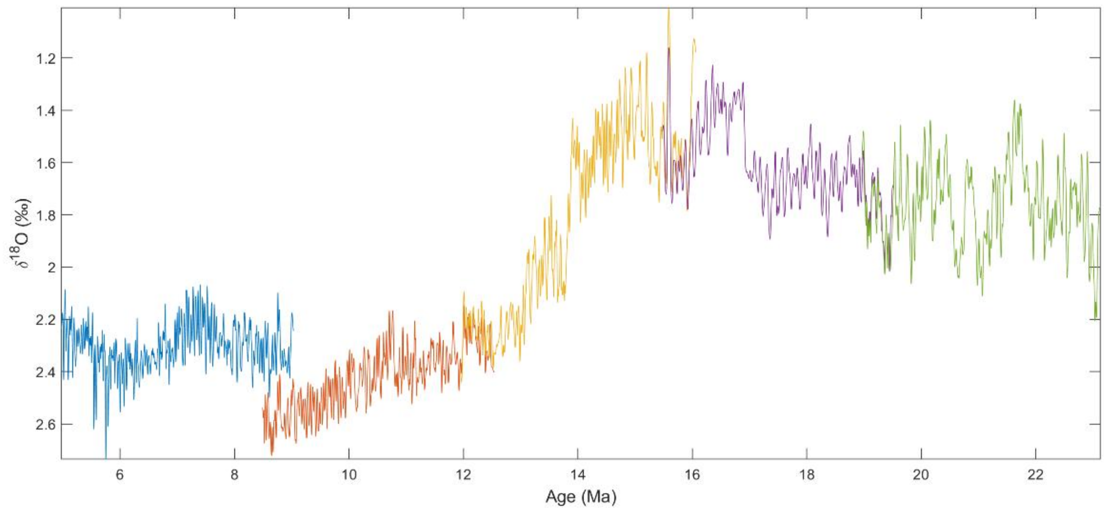


**Figure A1:** The five separate global stack segments (various colors) output by BIGMACS prior to applying offset corrections and stitching them together into a composite stack.

## Code, data, or code and data availability

BIGMACS input files, output files, final versions of the global and EEP stacks, and the Matlab code used to stitch together the global stack segments are archived on Zenodo (http://doi.org/10.5281/zenodo.21519959). [*Restricted access until publication*.]

## Author contributions

BH and LEL designed the experiments in consultation with CEL, TL and YZ. BH performed the experiments; BH and LEL analyzed the results. BH and LEL prepared the manuscript with contributions from all co-authors.

https://doi.org/10.5194/egusphere-2026-4648
Preprint. Discussion started: 12 August 2026


**Competing interests**

Editorship CI! The authors have the following competing interests: At least one of the (co-)authors is a member of the editorial board of Climate of the Past.

**Disclaimer**



**Acknowledgements**

This manuscript benefited from conversations with Francis Macdonald, David Lea, Thomas Westerhold, Anna Joy Drury, Stephen Meyers, and Samuel Newall. Use was made of computational facilities purchased with funds from the National Science Foundation (CNS-1725797) and administered by the Center for Scientific Computing (CSC). The CSC is supported by the California NanoSystems Institute and the Materials Research Science and Engineering Center (MRSEC; NSF DMR2308708) at UC Santa Barbara.

**Financial support**

This research has been supported by the Heising-Simons Foundation, grant no. 2021-2799 and by the National Science Foundation, the Directorate for Geosciences (grant no. EAR-1926001, OCE-1760838, OCE-1760878).

**Review statement**

The review statement will be added by Copernicus Publications listing the handling editor as well as all contributing referees according to their status anonymous or identified.

**References**

Abdul Aziz, H., Krijgsman, W., Hilgen, F.J., Wilson, D.S., and Calvo, J.P.: An astronomical polarity timescale for the late middle Miocene based on cyclic continental sequences, Journal of Geophysical Research, **108**, 2159. https://doi.org/10.1029/2002JB001818, 2003.

Andersson, C., and Jansen, E.: A Miocene (8-12 Ma) intermediate water benthic stable isotope record from the northeastern Atlantic, ODP Site 982, Paleoceanography, 18(1), 1013, https://doi.org/10.1029/2001PA000657, 2003

Backman, J., Raffi, I., Rio, D., and Fornaciari, E.: Biozonation and biochronology of Miocene through Pleistocene calcareous nannofossils from low and middle latitudes, Newsletters on Stratigraphy, **45**, 221-244. https://doi.org/10.1127/0078-0421/2012/0022, 2012.

Barker, P.F., and Burrell, J.: The opening of the Drake Passage, Marine Geology, **25**, 15–34. https://doi.org/10.1016/0025-3227(77)90045-7, 1977.

Beddow, H.M., Liebrand, D., Sluijs, A., Wade, B.S., and Lourens, L.J.: Global change across the Oligocene-Miocene transition: High-resolution stable isotope records from IODP Site U1334 (equatorial Pacific Ocean), *Paleoceanography, 31,* 81–97. https://doiorg.ezp.sub.su.se/10.1002/2015PA002820, 2016.

Bickert, T., Haug, G. H., and Tiedemann, R.: Late Neogene benthic stable isotope record of ODP Site 999: Implications for Caribbean paleoceanography, organic carbon burial and the Messininian Salinity Crisis, Paleoceanography, 19(1), PA1023, https://doi.org/10.1029/2002PA000799, 2004.

Billups, K., Channell, J.E.T., and Zachos, J.: Late Oligocene to early Miocene geochronology and paleoceanography from the subantarctic South Atlantic, Paleoceanography, 17, 4-1-4-11. https://doi.org/10.1029/2000PA000568, 2002.

Billups, K., Pälike, H., Channell, J. E. T., Zachos, J. C., and Shackleton, N. J.: (Appendix A1) Stable carbon and oxygen isotope ratios of benthic foraminifera from ODP Site 177-1090 [dataset], PANGAEA, https://doi.org/10.1594/PANGAEA.708067, 2004.

Bolton, C. T., Gray, E. , Kuhnt, W., Holbourn, A. E., Lübbers, J., Grant, K. M., Tachikawa, K., Marino, G., Rohling, E. J., Sarr, A.-C., and Andersen, N.: Late Miocene benthic stable isotope data, age model, and X-Ray Fluorescence data from IODP Site U1443, equatorial Indian Ocean [dataset bundled publication], PANGAEA, https://doi.org/10.1594/PANGAEA.935166, 2021.

Bradshaw, C.D., Lunt, D.J., Flecker, R., Salzmann, U., Pound, M.J., Haywood, A.M., and Eronen, J.T.: The relative roles of $CO_2$ and paleogeography in determining late miocene climate: Results from a terrestrial model–data comparison, Climate of the Past, 8, 1257–1285. https://doi.org/10.5194/cp-8-1257-2012, 2012.

Bradshaw, C.D., Lunt, D.J., Flecker, R., Salzmann, U., Pound, M.J., Haywood, A.M., and Eronen, J.T.: Corrigendum to "The relative roles of $CO_2$ and paleogeography in determining late Miocene climate: Results from a terrestrial model–data comparison," Climate of the Past, 10, 199–206, https://doi.org/10.5194/cp-10-199-2014, 2014.

Burls, N.J., Bradshaw, C.D., De Boer, A.M., Herold, N., Huber, M., Pound, M., Dannadieu, Y., Farnsworth, A., Frigola, A., Gasson, E., von der Heydt, A.S., Hutchinson, D.K., Knorr, G., Lawrence, K.T., Lear, C.H., Li, X., Lohmann, G., Lunt, D.J., Marzocchi, A., Prange, M., Riihimaki, C.A., Sarr, A.-C., Siler, N., and Zhang, Z.: Simulation Miocene warmth: Insights from an opportunistic multi-model ensemble (MioMIP1), Paleoceanography and Paleoclimatology, 36, e2020PA004054. https://doi.org/10.1029/2020PA004054, 2021.

Butzin, M., Lohmann G., and Bickert, T.: Miocene ocean circulation inferred from marine carbon cycle modeling combined with benthic isotope records, Paleoceanography, 26, https://doi.org/10.1029/2009PA001901, 2011.

Christensen, B.A., Renema, W., Henderiks, J., De Vleeschouwer, D., Groeneveld, J., Castañeda, I.S., Reuning, L., Bogus, K., Auer, G., Ishiwa, T., McHugh, C.M., Gallagher, S.J., Fulthorpe, C.S., and IODP Expedition 356 Scientists: Indonesian Throughflow drove Australian climate from humid Pliocene to arid Pleistocene, Geophysical Research Letters, 44, 6914-1925, https://doi.org/10.1002/2017GL072977, 2017.

Cramer, B.S., Toggweiler, J.R., Wright, J.D., Katz, M.E., and Miller, K.G.: Ocean overturning since the Late Cretaceous: Inferences from a new benthic foraminiferal isotope compilation. Paleoceanography, 24, https://doi.org/10.1029/2008PA001683, 2009.

De Vleeschouwer, D., Vahlenkamp, M., Crucifix, M., and Pälike, H.: Alternating Southern and Northern Hemisphere climate response to astronomical forcing during the past 35 m.y. Geology, 45 (4), 375– 378, https://doi.org/10.1130/G38663.1, 2017.

Dickens, G.R., and Owen, R.M.: The latest Miocene-early Pliocene biogenic bloom: A revised Indian ocean perspective, Marine Geology, 161, 75–91, https://doi.org/10.1016/S0025-3227(99)00057-2, 1999.

Ding, L., Spicer, R. A., Yang, J., Xu, Q., Cai, F., Li, S., Lai, Q., Wang, H., Spicer, T.E.V., Yue, Y., Shukla, A., Srivastava, G., Khan, M.A., Bera, S., and Mehrotra, R.: Quantifying the rise of the Himalaya orogen and implications for the South Asian monsoon, Geology, 45, 215–218. https://doi.org/10.1130/G38583.1, 2017.

Drury, A. J., Liebrand, D., Westerhold, T., Beddow, H. B., Hodell, D. A., Rolfs, N., Wilkens, R. H., Lyle, M., Bell, D. B., Kroon, D., Pälike, H., and Lourens, L. J.: Climate, cryosphere and carbon cycle controls on Southeast Atlantic orbital-scale carbonate deposition since the Oligocene (30-0 Ma), Climate of the Past, 17(5), 2091-2117, https://doi.org/10.5194/cp-17-2091-2021, 2021.

Drury, A.J., Westerhold, T., Frederichs, T., Tian, J., Wilkens, R., Channell, J.E.T., Evans, H., John, C.M., Lyle, M., Röhl, U. (2017). Late Miocene climate and time scale reconciliation: Accurate orbital calibration from a deep-sea perspective, Earth and Planetary Science Letters, 475, 254-266, https://doi.org/10.1016/j.epsl.2017.07.038, 2017.

Ehlers, B.M., and Jokat, W.: Paleo-bathymetry of the northern North Atlantic and consequences for the opening of the Fram Strait, Marine Geophysical Research, 34, 25–43, https://doi.org/10.1007/s11001-013-9165-9, 2013.

Evangelinos, D., Etourneau, J., van de Flierdt, T., Crosta, X., Jeandel, C., Flores, J.-A., Harwood, D.M., Valero, L., Ducassou, E., Sauermilch, I., Klocker, A., Cacho, I., Pena, L.D., Kreissig, K., Benoit, M., Belhadj, M., Paredes, E., Garcia-Solsona, E., López-Quirós, A., Salabarnada, A., Escutia, C.: Late Miocene onset of the modern Antarctic Circumpolar Current, Nature Geoscience, 17, 165-170, https://doi.org/10.1038/s41561-023-01356-3, 2024.

Flower, B.P., Kennett, J.P.: Middle Miocene ocean-climate transition: High-resolution oxygen and carbon isotopic records from Deep Sea Drilling Project Site 588A, southwest Pacific, Paleoceanography, 8, 811-843. https://doi.org/10.1029/93PA02196, 1993.

Foster, G.L., Lear, C.H., Rae, J.W.B.: The evolution of $pCO_2$, ice volume and climate during the middle Miocene, Earth and Planetary Science Letters, 341, 243–254. https://doi.org/10.1016/j.epsl.2012.06.007, 2012.

https://doi.org/10.5194/egusphere-2026-4648
Preprint. Discussion started: 12 August 2026


Galeotti, S., DeConto, R., Naish, T., Stocchi, P., Florindo, F., Pagani, M., Barrett, P., Bohaty, S.M., Lanci, L., Pollard, D., Sandroni, S., Talarico, F.M., and Zachos, J.C.: Antarctic Ice Sheet variability across the Eocene-Oligocene boundary climate transition, Science, 352, 76–80. https://doi.org/10.1126/science.aab0669, 2016.

Gastaldello, M. E., Agnini, C., Westerhold, T., Drury, A. J., Sutherland, R., Drake, M. K., Lam, A. R., Dickens, G. R., Dallanave, E., Burns, S. J., and Alegret, L.: Stable isotope ($\delta^{13}C$, $\delta^{18}O$) of *Cibicides mundulus* from IODP Hole 371-U1506A [dataset]. PANGAEA, https://doi.org/10.1594/PANGAEA.953684, 2023.

Gladenkov, A.Y., and Gladenkov, Y.B.: Onset of connections between the Pacific and Arctic oceans through the Bering Strait in the Neogene, Stratigraphy and Geological Correlation, 12, 175–187, 2004.

Goldner, A., Herold, N., and Huber, M.: The challenge of simulating the warmth of the mid-Miocene climatic optimum in CESM1, Climate of the Past, 10, 523–536. https://doi.org/10.5194/cp-10-523-2014, 2014.

Haug, G.H., Tiedemann, R., Zahn, R., and Ravelo, A.C.: Role of Panama uplift on oceanic freshwater balance, Geology, 29, 207–210, https://doi.org/10.1130/0091-7613(2001)029<0207:ROPUOO>2.0.CO;2, 2001.

Haq, B.U.: Biogeographic history of Miocene calcareous nannoplankton and paleoceanography of the Atlantic Ocean, Micropaleontology, 26, 414-443. https://doi.org/10.2307/1485353, 1980.

Henderiks, J., Bartol, M., Pige, N., Karatsolis, B.-Th., and Lougheed, B.C.: Shifts in phytoplankton composition and stepwise climate change during the middle Miocene, Paleoceanography and Paleoclimatology, 35, e2020PA003915. https://doi.org/10.1029/2020PA003915, 2020.

Herbert, T.D., Dalton, C.A., Liu, Z., Salazar, A., Si, W., and Wilson, D.S.: Tectonic degassing drove global temperature trends since 20 Ma, Science, 377, 116-119. https://doi.org/10.1126/science.abl4353, 2022.

Herold, N., Huber, M., Greenwood, D.R., Müller, R.D., and Seton, M.: Early to middle Miocene monsoon climate in Australia, Geology, 39, 3–6, https://doi.org/10.1130/G31208.1, 2011.

Herold, N., Huber, M., Müller, R.D., and Seton, M.: Modeling the Miocene climatic optimum: Ocean circulation. Paleoceanography, 27, PA1209, https://doi.org/10.1029/2010pa002041, 2012.

Hobart, B., Zhou, Y., Lee, T. Lawrence, C. E., and Lisiecki, L. E.: Supporting information for "Quantifying trends and transitions in a Miocene benthic $\delta^{18}O$ stack," Zenodo [data set], https://doi.org/10.5281/zenodo.21519959, 2026.

Hodell, D.A., and Kennett, J.P.: Late Miocene–Early Pliocene stratigraphy and paleoceanography of the South Atlantic and southwest Pacific oceans: A synthesis, Paleoceanography, 1, 285-311. https://doi.org/10.1029/PA001i003p00285, 1986.

Hodell, D.A., and Woodruff, F.: Variations in the strontium isotopic ratio of seawater during the Miocene: Stratigraphic and geochemical implications, Paleoceanography, 9, 405-426, https://doi.org/10.1029/94PA00292, 1994.

Holbourn, A. E., Kuhnt, W., Schulz, M., Flores, J.-A., and Andersen, N.: Orbitally-paced climate evolution during the middle Miocene "Monterey" carbon-isotope excursion, Earth and Plan. Sci. Lett., 261, 534– 550. http://dx.doi.org/10.1016/j.epsl.2007.07.026, 2007.

Holbourn, A. E., W. Kuhnt, M. Lyle, L. Schneider, O. Romero, and Andersen, N.: Middle Miocene climate cooling linked to intensification of eastern equatorial Pacific upwelling, Geology, **42**, 19–22, doi:10.1130/G34890.1, 2014.

Holbourn, A.E., Kuhnt, W., Kochhann, K.G.D., Andersen, N., and Meier, K.J.S.: Global perturbation of the carbon cycle at the onset of the Miocene climatic optimum, Geology, 43, 123– 126, https://doi.org/10.1130/G36317.1, 2015.

Holbourn, A. E., Kuhnt, W., Clemens, S. C., Kochhann, K. G. D., Jöhnck, J., Lübbers, J., and Andersen, N.: Late Miocene climate cooling and intensification of southeast Asian winter monsoon, Nature Communications, 9, 1584, https://doi.org/10.1038/s41467-018-03950-1, 2018.

Holbourn, A. E., Kuhnt, W., Clemens, S. C., and Heslop, D.: Benthic and planktic foraminiferal isotope data from ODP Site 184-1146 [dataset]. PANGAEA, https://doi.org/10.1594/PANGAEA.931108, 2021.

Holbourn, A. E., Kuhnt, W., Kochhann, K. G. D., Matsuzaki, K. M., and Andersen, N.: Middle Miocene climate-carbon cycle dynamics: keys for understanding future trends on awarmer Earth?, in: Understanding the Monterey Formation and Similar Biosiliceous Units Across Space and Time, edited by: Aiello, I., Barron, J. and Ravelo, C., Geological Society of America, Special Paper 556, 1–19, 2022.

Holbourn, A. E., Kuhnt, W., Kulhanek, D.K.: Stable isotope record on revised age model, ODP Hole 189-1171C [dataset], PANGAEA, https://doi.org/10.1594/PANGAEA.972494, 2024.

Hönish, B., Royer, D.L., Breecker, D.O., Polissar, P.J., Bowen, G.J., Henehan, M., Cui, Y., Steinthorsdottir, M., McElwain, J.C., Kohn, M.J., Pearson, A., Phelps, S.R., Uno, K. T., Ridgwell, A., Anagnostou, E., Austermann, J., Badger, M.P.S., Barclay, R.S., Bijl, P. K., Chalk, T.B., Scotese, C.R., de la Vega, E., DeConto, R.M., Dyez, K.A., Ferrini, V., Franks, P.J., Giulivi, C.F., Gutjahr, M., Harper, D.T., Haynes, L.L., Huber, M., Snell, K. E., Keisling, B.A., Konrad, W., Lowenstein, T.K., Malinverno, A., Guillermic, M., Mejía, L.M., Milligan, J.N., Morton, J.J., Nordt, L., Whiteford, R., Roth-Nebelsick, A., Rugenstein, J.K.C., Schaller, M.F., Sheldon, N.D., Sosdian, S., Wilkes, E.B., Witkowski, C.R., Zhang, Y.G., Anderson, L., Beerling, D.J., Bolton, C., Cerling, T.E., Cotton, J.M., Da, J., Ekart, D.D., Foster, G.L., Greenwood, D.R., Hyland, E.G., Jagniecki, E.A., Jasper, J.P., Kowalczyk, J.B., Kunzmann, L., Kürschner, W.M., Lawrence, C.E., Lear, C.H., Martínez-Botí, M. A., Maxbauer, D.P., Montagna, P., Naafs, B.D.A., Rae, J.W.B., Raitzsch, M., Retallack, G.J., Ring, S.J., Seki, O., Sepúlveda, J., Sinha, A., Tesfamichael, T.F., Tripati, A., van der Burgh, J., Yu, J., Zachos, J.C., and Zhang, L.: Toward a Cenozoic history of atmospheric $CO_2$. Science, 382, 6675. https://doi.org/10.1126/science.adi5177, 2023.

Hossain, A., Knorr, G., Jokat, W. and Lohmann, G.: Opening of the fram Strait led to the establishment of a modern-like three-layer stratification in the Arctic Ocean during the Miocene, Arktos, **7**, 1-12. https://doi.org/10.1007/s41063-020-00079-8, 2021.

Huang, Y., Chen, C., Bai, Y., Fang, X., Song, L., and Li, Y.: Late Miocene cooling and uplift recorded by bacterial H-GDGTs in the Xining Basin, northeastern Tibetan Plateau, Palaeogeography, Palaeoclimatology, Palaeoecology, 650, 112354. https://doi.org/10.1016/j.palaeo.2024.112354, 2024.

Jagoutz, O., Macdonald, F.A., and Royden, L.: Low-latitude arc-continent collision as a driver for global cooling, Proceedings of the National Academy of Sciences, 113, 4935-4940, https://doi.org/10.1073/pnas.1523667113, 2016.

Jiang, P., Yu, G., Zhang, Q., Zou, Y., Tang, Q., Kang, Z., Sytharith, P., and Xiao, H.: Chemical weathering and $CO_2$ consumption rates of rocks in the Bishuiyan subterranean basin of Guangxi, China, Scientific Reports, 10, 11677. https://doi.org/10.1038/s41598-020-68572-4, 2020.

Jöhnck, J., Wolfgang, W., Holbourn, A. E., and Andersen, N.: Benthic and planktic foraminiferal carbon and oxygen isotopes and Mg/Ca-derived mixed layer temperatures from IODP Hole 353-U1448A and 353-U1448B in the Andaman Sea [dataset], PANGAEA, https://doi.org/10.1594/PANGAEA.921091, 2020.

Kasbohm, J., Schoene, B., Montanari, A., and Coccioni, R.: High-precision U-Pb zircon geochronology of the Miocene Bisciaro Formation, Contessa Section, Italy: A case study for requisite radioisotopic calibration of bio- and magnetostratigraphy, Palaeogeo. Palaeoclim. Palaeoeco., 576, 110487. https://doi.org/10.1016/j.palaeo.2021.110487, 2021.

Kasbohm, J., Schoene, B., Thomas, E., and Hull, P.: High-precision U-Pb geochronology for the Miocene Climatic Optimum & a novel approach for calibrating age models in deep-sea sediment cores, Geology, 52, 747–752, https://doi.org/10.1130/G52255.1, 2024.

Keigwin, L.: Isotopic paleoceanography of the Caribbean and east pacific: Role of Panama uplift in late Neogene time, Science, 217, 350–353. https://doi.org/10.1126/science.217.4557.350, 1982.

Kirillova, V., Osborne, A. H., Störling, T., and Frank, M.: Miocene restriction of the Pacific-North Atlantic throughflow strengthened Atlantic overturning circulation, Nature Communications, 10, 1–7. https://doi.org/10.1038/s41467-019-12034-7, 2019.

Kissel, C., Laj, C., Clemens, S., and Solheid, P.: Magnetic signature of environmental changes in the last 1.2 Myr at ODP Site 1146, South China Sea, Marine Geology, 201, 119-132, https://doi.org/10.1016/S0025-3227(03)00212-3, 2003.

Kochhann, K.G.D., Holbourn, A., Kuhnt, W., Channell, J.E.T., Lyle, M., Shackford, J.K., Wilkens, R.H., and Andersen, N.: Eccentricity pacing of eastern equatorial Pacific carbonate dissolution cycles during the Miocene Climatic Optimum, Paleoceanography, 31, 1176-1192. https://doi.org/10.1002/2016PA002988, 2016.

Kochhann, K. G. D., Kuhnt, W., Holbourn, A. E., Usui, Y., Lübbers, J., Beil, S., and Andersen, N.: Stable carbon and oxygen isotope measurements of Cibicidoides wuellerstorfi and C. mundulus from IODP Site 353-U1443 [dataset], PANGAEA, https://doi.org/10.1594/PANGAEA.926838, 2021.

Krapp, M., and Jungclaus, J. H.: The Middle Miocene climate as modeled in an atmosphere-ocean-biosphere model, Climate of the Past, 7, 1169–1188, https://doi.org/10.5194/cp-7-1169-2011, 2011.

Kuhnt, W., Holbourn, A. E., Hall, R., Zuvela, M., and Käse, R.: Neogene history of the Indonesian throughflow. Continent-Ocean Interactions within East Asian Marginal Seas, Geophysical Monograph, 149, 299–320, https://doi.org/10.1029/149GM16, 2004.

Kryolov, A.A., Andreeva, I.A., Vogt, C., Backamn, J., Krupskaya, V.V., Grikurov, G.E., Moran, K., and Shoji, H.: A shift in heavy and clay mineral provenance indicates a middle Miocene onset of a perennial sea ice cover in the Arctic Ocean, Paleoceanography, 23, https://doi.org/10.1029/2007PA001497, 2008.

https://doi.org/10.5194/egusphere-2026-4648
Preprint. Discussion started: 12 August 2026


Lagabrielle, Y., Godderis, Y., Donnadieu, Y., Malavieille, J., and Suarez, M. : The tectonic history of Drake Passage and its possible impacts on global climate, Earth Plan. Sci. Lett., 279, 197-211, https://doi.org/10.1016/j.epsl.2008.12.037, 2009.

Laskar, J., Fienga, A., Gastineau, M., and Manche, H.: La2010: a new orbital solution for the long-term motion of the Earth, Astronomy and Astrophysics, 532, A89. https://doi.org/10.1051/0004-6361/201116836, 2011.

Lear, C. H., Coxall, H. K., Foster, G. L., Lunt, D. J., Mawbey, E., Rosenthal, Y., Sosdian, S. M., Thomas, E., Wilson, P. A.: Neogene ice volume and ocean temperatures: Insights from infaunal foraminiferal Mg/Ca paleothermometry, Paleoceanography, 30, 1437–1454. https://doi.org/10.1002/2015PA002833, 2015

Lee, T., Rand, D., Lisiecki, L.E., Gebbie, G., Lawrence, C.: Bayesian age models and stacks: combining age inferences from radiocarbon and benthic $\delta^{18}O$ stratigraphic alignment, Climate of the Past, 19, 1993-2012, https://doi.org/10.5194/cp-19-1993-2023, 2023.

Liebrand, D., H. M. Beddow, L. J. Lourens, H. Pälike, I. Raffi, S. M. Bohaty, F. J. Hilgen, M. J. M. Saes, P. A. Wilson, A. E. van Dijk, D. A. Hodell, D. Kroon, Huck, C. E., and Batenburg, S. J.: Cyclostratigraphy and eccentricity tuning of the early Oligocene through early Miocene (30.1–17.1 Ma): Cibicides mundulus stable oxygen and carbon isotope records from Walvis Ridge Site 1264, Earth Planet. Sci. Lett., 450, 392–405. doi:10.1016/j.epsl.2016.06.007, 2016.

Liebrand, D., de Bakker, A. T. M., Beddow, H. M., Wilson, P. A., Bohaty, S. M., Ruessink, G., et al.: Evolution of the early Antarctic ice ages. Proc. Nat. Academy of Sciences, 114 (15), 3867, https://doi.org/10.1073/pnas.1615440114, 2017.

Lisiecki, L. E., and Raymo, M. E.: A Pliocene–Pleistocene stack of 57 globally distributed benthic $\delta^{18}O$ records, Paleoceanography, 20, PA1003, https://doi.org/10.1029/2004PA001071, 2005.

Liu, F., Dua, J., Huang, E., Mab, W., Mac, X., Lourens L. J., and Tian, J.: Accelerated marine carbon cycling forced by tectonic degassing over the Miocene Climate Optimum, Science Bulletin, 69, 823–832, https://doi.org/10.1016/j.scib.2023.12.052, 2024.

Liu, X., and Dong, B.: Influence of the Tibetan Plateau uplift on the Asian monsoon-arid environment evolution, Chinese Science Bulletin, 58, 4277-4291, https://doi.org/10.1007/s11434-013-5987-8, 2013.

Liu, Z.-C., Wang, J.-G., Liu, X.-C., Liu, Y., and Lai, Q.-Z.: Middle Miocene ultrapotassic magmatism in the Himalaya: A response to mantle unrooting process beneath the orogen, Terra Nova, 33, 240-251, https://doi.org/10.1111/ter.12507, 2021.

Lyle, M., Drury, A.J., Tian, J., Wilkens, R., and Westerhold, T.: Late Miocene to Holocene high-resolution eastern equatorial Pacific carbonate records: Stratigraphy linked by dissolution and paleoproductivity, Clim. Past, 15, 1715-1739. https://www.clim-past.net/15/1715/2019/, 2019.

Ma, X., Tian, J., Ma, W., Li, K., and Yu, J.: Changes of deep Pacific overturning circulation and carbonate chemistry during middle Miocene East Antarctic ice sheet expansion, Earth Plan. Sci. Lett., 484, 253-263, https://doi.org/10.1016/j.epsl.2017.12.002, 2018.

Macdonald, F.A., Swanson-Hysell, N.L., Park, Y., Lisiecki, L., and Jagoutz, O.: Arc-continent collisions in the tropics set Earth's climate state, Science, 364, 181-184, https://doi.org/10.1126/science.aav5300, 2019.

https://doi.org/10.5194/egusphere-2026-4648
Preprint. Discussion started: 12 August 2026


Micheels, A., Bruch, A.A., Eronen, J., Fortelius, M., Harzhauser, M., Utescher, T., and Mosbrugger, V.: Analysis of heat transport mechanisms from a Late Miocene model experiment with a fully-coupled atmosphere–ocean general circulation model, Palaeogeography Palaeoclimatology Palaeoecology, 304, 337–350, https://doi.org/10.1016/j.palaeo.2010.09.021, 2011.

Miller, K.G., Baluyot, R., Wright, J.D., Kopp, R.E., and Browning, J.V.: Closing an early Miocene astronomical gap with Southern Ocean $\delta^{18}O$ and $\delta^{13}C$ records: Implications for sea level change, Paleoceanography, 32, 600-621, https://doi.org/10.1002/2016PA003074, 2017.

Miller, K.G., Browning, J.V., Schmelz, W.J., Kopp, R.E., Mountain, G.S., and Wright, J.D.: Cenozoic sea-level and cryospheric evolution from deep-sea geochemical and continental margin records, Science Advances, 6, eaaz1346. https://doi.org/ 10.1126/sciadv.aaz1346, 2020.

Molnar, P., and England, P.: Late Cenozoic uplift of mountain ranges and global climate change: chicken or egg?, Nature, 346, 29-34, https://doi.org/10.1038/346029a0, 1990.

Montes, C., Cardona, A., Jaramillo, C., Pardo, A., Silva, J. C., Valencia, V., Ayala, C., Pérez-Angel, L. C., Rodriguez-Parra, L. A., Ramirez, V., and Niño, H.: Middle Miocene closure of the central American seaway, Science, 348, 226–229, https://doi.org/10.1126/science.aaa2815, 2015.

Morée, A. L., Sun, T., Bretones, A., Straume, E. O., Nisancioglu, K., and Gebbie, G.: Cancellation of the precessional cycle in $\delta^{18}O$ records during the Early Pleistocene, Geophysical Research Letters, 48, e2020GL090035, https://doi.org/10.1029/2020GL090035, 2021.

O'Dea, A., Lessios, H. A., Coates, A. G., Eytan, R. I., Restrepo-Moreno, S. A., Cione, A. L., et al.: Formation of the isthmus of Panama, Science Advances, 2, e1600883, https://doi.org/10.1126/sciadv.1600883, 2016.

Pälike, H., Norris, R. D., Herrle, J. O., Wilson, P. A., Coxall, H. K., Lear, C. H., et al.: The heartbeat of the Oligocene climate system, Science, 314, 1894– 1898, https://doi.org/10.1126/science.1133822, 2006.

Pekar, S. F., and DeConto, R. M.: High-resolution ice-volume estimates for the early Miocene: Evidence for a dynamic ice sheet in Antarctica, Palaeogeography Palaeoclimatology Palaeoecology, 231, 101–109, https://doi.org/10.1016/j.palaeo.2005.07.027, 2007.

Rae, J.W.B., Zhang, Y.G., Liu, X., Foster, G.L., Stoll, H.M., and Whiteford, R.D.M.: Atmospheric $CO_2$ over the past 66 million years from marine archives, Annual Review of Earth and Planetary Sciences, 49, 609-641,https://doi.org/10.1146/annurev-earth-082420-063026, 2021.

Raitzsch, M., Bijma, J., Bickert, T., Schulz, M., Holbourn, A., Kučera, M. (2021). Atmospheric carbon dioxide variations across the middle Miocene climate transition. *Climate of the Past*, **17**, 703-719. https://doi.org/10.5194/cp-17-703-2021

Raymo, M. E., and Ruddiman, W. F.: Tectonic forcing of late Cenozoic climate, Nature, 359, 117-122, https://doi.org/10.1038/359117a0, 1992.

Rio, D., Raffi, I., and Villa, G.: Pliocene-Pleistocene calcareous nannofossil distribution patterns in the Western Mediterranean, Proceedings of the Ocean Drilling Program, Scientific Results, 107, https://10.2973/odp.proc.sr.107.164.1990, 1990.

Rögl, F.: Mediterranean and Paratethys. Facts and hypotheses of an Oligocene to Miocene paleogeography (short overview), Geologica Carpathica, 50, 339–349, 1999.

Rowley, D. B., and Garzione, C. N.: Stable isotope-based paleoaltimetry, Annual Review of Earth and Planetary Sciences, 35, 463–508, https://doi.org/10.1146/annurev.earth.35.031306.140155, 2007.

Ruddiman, W.F., Raymo, M.E., Prell, W.L., and Kutzbach, J.E: Uplift-climate connection: a synthesis, In: Tectonic Uplift and Climate Change. Edited by: Ruddiman, W. F., Springer, Boston, MA. https://doi.org/10.1007/978-1-4615-5935-1_20, 1997.

Ruggieri, E., and Lawrence, C.E.: The Bayesian change point and variable selection algorithm: application to the $\delta^{18}O$ proxy record of the Plio-Pleistocene, Journal of Computational and Graphical Statistics, 23, 87-110, https://doi.org/10.1080/10618600.2012.707852, 2014.

Shackleton, N. J., Crowhurst, S. J., Weedon, G. P., and Laskar, J.: Astronomical calibration of Oligocene-Miocene time, Philosophical Transactions of the Royal Society A, London, 357, 1907– 1929, https://doi.org/10.1098/rsta.1999.0407, 1999.

Shackleton, N. J., and Hall, M. A.: The Late Miocene stable isotope record, Site 926, In: Proceedings of the Ocean Drilling Program, Scientific Results, Edited by: Shackleton, N.J., Curry, W.B., Richter, C., and Bralower, T.J., 154, 367-373, 1997.

Shevenell, A. E., and Kennett, J. P.: Paleoceanographic change during the Middle Miocene climate revolution: An Antarctic stable isotope perspective. In: The Cenozoic Southern Ocean: Tectonics, Sedimentation, and Climate Change Between Australia and Antarctica, Edited by: Exon, N. F., Kennett, J. P., Malone, M. J., Geophysical Monograph Series, 151, American Geophysical Union, Washington, D. C., 235-251, https://doi.org/10.1029/151GM14, 2004.

Simon, D., Palcu, D., Meijer, P., and Krijgsman, W.: The sensitivity of middle Miocene paleoenvironments to changing marine gateways in Central Europe, Geology, 47, 35–38, https://doi.org/10.1130/G45698.1, 2018.

Sosdian, S.M., Babila, T.L., Greenop, R., Foster, G.L., and Lear, C.H.: Ocean carbon storage across the middle Miocene: A new interpretation for the Monterey event, Nature Communications, 11, 134, https://doi.org/10.1038/s41467-019-13792-0, 2020.

Steinthorsdottir, M., Jardine, P.E., and Rember, W.C.: Near-future $pCO_2$ during the hot Miocene Climatic Optimum, Paleoceanography and Paleoclimatology, 36, e2020PA003900, https://doi.org/10.1029/2020PA003900, 2020.

Steinthorsdottir, M., Coxall, H.K., de Boer, A.M., Huber, M., Barbolini, N., Bradshaw, C.D., Burls, N.J., Feakins, S.J., Gasson, E., Henderiks, J., Holbourn, A. E., Kiel, S., Kohn, M. J., Knorr, G., Kürschner, W. M., Lear, C. H., Liebrand, D., Lunt, D. J., Mörs, T., Pearson, P. N., Pound, M. J., Stoll, H., and Strömberg, C. A. E.: The Miocene: The future of the past. Paleoceanography and Paleoclimatology, 36, e2020PA004037, https://doi.org/10.1029/2020PA004037, 2021.

Steph, S.: Oxygen and carbon isotope ratios of foraminifers of ODP Site 165-1000 [dataset], PANGAEA, https://doi.org/10.1594/PANGAEA.272449, 2005.

Super, J.R., Thomas, E., Pagani, M., Huber, M., O'Brien, C., and Hull, P.M.: North Atlantic temperature and $pCO_2$ coupling in the early-middle Miocene, Geology, 46, 519–522. https://doi.org/10.1130/G40228.1, 2018.

https://doi.org/10.5194/egusphere-2026-4648
Preprint. Discussion started: 12 August 2026


The MathWorks Inc., MATLAB version: R2024b, Natick, Massachusetts: The MathWorks Inc., https://www.mathworks.com (last access: March 2025), 2024

Thomas, D.J., and Via, R.K.: Neogene evolution of Atlantic thermohaline circulation: Perspective from Walvis Ridge, southeastern Atlantic Ocean, Paleoceanography, 22, https://doi.org/10.1029/2006PA001297, 2007.

Tian, J., Yang, M., Lyle, M.W., Wilkens, R., and Shackford, J.K.: Obliquity and long eccentricity pacing of the Middle Miocene climate transition, Geochemistry Geophysics Geosystems, 14, 1740–1755, https://doi.org/10.1002/ggge.20108, 2013.

Tiedemann, R., Sturm, A., Steph, S., Lund, S. P., and Stoner, J. S.: Astronomically calibrated timescales from 6 to 2.5 Ma and benthic isotope stratigraphies, Sites 1236, 1237, 1239, and 1241. In: Proceedings of the Ocean Drilling Program, Scientific Results, Edited by: Tiedemann, R; Mix, AC; Richter, C; Ruddiman, WF College Station, TX (Ocean Drilling Program), 202, 1-69, https://doi.org/10.2973/odp.proc.sr.202.210.2007, 2007.

Toggweiler, J.R., and Bjornsson, H.: Drake Passage and paleoclimate, Journal of Quaternary Science, 15, 319-328, https://doi.org/10.1002/1099-1417(200005)15:4<319::AID-JQS545>3.0.CO;2-C, 2000.

Tripati, A.K., Elderfield, H. Booth, L., Zachos, J. C., and Ferretti, P.: Data report: High-resolution benthic foraminiferal stable isotope stratigraphy across the Oligocene/Miocene boundary at Site 1218, In: Proceedings of the Ocean Drilling Program, Scientific Results, Edited by: Wilson, PA; Lyle, M; Firth, JV, College Station, TX (Ocean Drilling Program), 199, 1-13, https://doi.org/10.2973/odp.proc.sr.199.221.2006, 2006.

Voigt, J., Hathorne, E., Frank, M., and Holbourn A. E.: Miocene stable isotope record of benthic foraminifera from IODP Site 320-U1336 [dataset], PANGAEA, https://doi.org/10.1594/PANGAEA.854835, 2015.

Wang, C. S., Dai, J., Zhao, X., Li, Y., Graham, S. A., He, D., Ran, B., and Meng, J.: Outward-growth of the Tibetan plateau during the Cenozoic: A review, Tectonics, 621, 1–43, https://doi.org/10.1016/j.tecto.2014.01.036, 2014.

Wang, D., Roberts, A.P., Rohling, E.J., Yao, W., Zhong, Y., Yao, Z., Lu, Y., and Liu, Q.: Equatorial Pacific dust fertilization and source weathering influences on Eocene to Miocene global $CO_2$ decline, Communications Earth & Environment, 4, 37, https://doi.org/10.1038/s43247-023-00702-y, 2023.

Westerhold, T., Agnini, C., Anagnostou, E., Hilgen, F., Hönisch, B., Meckler, A. N., Pälike, H., Wade, B., Sosdian, S., and Kasbohm, J.: Timing is everything, Paleoceanography and Paleoclimatology, 39, e2024PA004932. https://doi.org/10.1029/2024PA004932, 2024.

Westerhold, T., Bickert, T., and Röhl, U.: Middle to late Miocene oxygen isotope stratigraphy of ODP site 1085 (SE Atlantic): new constrains on Miocene climate variability and sea-level fluctuations, Palaeogeography, Palaeoclimatology, Palaeoecology, 217, 205-222, https://doi.org/10.1016/j.palaeo.2004.12.001, 2005.

Westerhold, T., Marwan, N., Drury, A. J., Liebrand, D., Agnini, C., Anagnostou, E., Barnet, J. S., Bohaty, S. M., De Vleeschouwer, D., and Florindo, F.: An astronomically dated record of Earth's climate and its predictability over the last 66 million years, Science, 369 (6509), 1383– 1387, https://doi.org/10.1126/science.aba6853, 2020.

Wilkens, R. H., Westerhold, T., Drury, A. J., Lyle, M. W., Gorgas, T. J., Tian, J.: Stable isotopes of ODP Site 154-926 [dataset], PANGAEA, https://doi.org/10.1594/PANGAEA.871108, 2017.

https://doi.org/10.5194/egusphere-2026-4648
Preprint. Discussion started: 12 August 2026


Woodruff, F., and Savin, S.M.: Miocene deepwater oceanography, Paleoceanography, 4, 87-140, https://doi.org/10.1029/PA004i001p00087, 1989.

Woodruff, F., and Savin, S.: Mid-Miocene isotope stratigraphy in the deep sea: High-resolution correlations, paleoclimatic cycles, and sediment preservation, Paleoceanography, 6, 755-806, https://doi.org/10.1029/91PA02561, 1991.

Wright, J. D., and Miller, K. G.: Control of north Atlantic deep water circulation by the Greenland-Scotland Ridge, Paleoceanography, 11, 157–170, https://doi.org/10.1029/95PA03696, 1996.

Zhang, L., Chen, M., Xiang, R., Zhang, L., and Lu, J.: Productivity and continental denudation history from the South China Sea since the late Miocene, Marine Micropaleontology, 72, 76-85, https://doi.org/10.1016/j.marmicro.2009.03.006, 2007.

Zhang, Y.G., Pagani, M., Liu, Z., Bohaty, S., and DeConto, R.: A 40-million-year history of atmospheric $CO_2$. *Philosophical Transactions of the Royal Society of London*, **371**, 20130096. https://doi.org/10.1098/rsta.2013.0096, 2013.

Zhou, Y., Lisiecki, L. E., Lee, T., Gebbie, G., and Lawrence, C.: Regional benthic $\delta^{18}O$ stacks for the "41-kyr world" – An Atlantic-Pacific divergence between 1.8 and 1.9 Ma, Geophysical Research Letters, 51, e2023GL107858, https://doi.org/10.1029/2023GL107858, 2024.